RSC Advances

PAPER

View Article Online
View Journal | View Issue

Cite this: *RSC Adv.*, 2020, **10**, 28454

Electrochemical oxidation of resorcinol: mechanistic insights from experimental and computational studies†

Kamonwad Ngamchuea, *[a] Bunrat Tharat,[a] Pussana Hirunsit[bc] and Suwit Suthirakun [ac]

This work investigates the mechanisms of resorcinol oxidation by density functional theory (DFT) calculation and cyclic voltammetry measurements. Complementary data from experimental and computational studies provide new insights into the reaction mechanisms. At both macro- and micro-electrodes, cyclic voltammetry of resorcinol is chemically and electrochemically irreversible over the whole pH range (1–14). Resorcinol molecules undergo a $1H^+$ $1e^-$ oxidation at pH < pK_{a1} and a $1e^-$ oxidation at pH > pK_{a2} to form radicals. The radicals then readily react to form dimers/polymers deposited on the electrode surface. All of the experimental findings are consistent with the proposed mechanisms, including the apparent transfer coefficient (β) of 0.6 ± 0.1, the slope of the peak potential (E_p) against pH of −54 mV pH^{-1}, the peak-shaped responses at micro-electrodes, and the fouling of the electrodes upon the oxidation of resorcinol. DFT calculation of the reaction energy of elementary steps and the eigenvalues of the highest occupied molecular orbital (HOMO) of the radical intermediates confirms that the ($1H^+$) $1e^-$ oxidation is the energetically favorable pathway. In addition to mechanistic insights, an electrochemical sensor is developed for resorcinol detection at microelectrodes in low ionic strength samples with the sensitivity of 123 ± 4 nA μM^{-1} and the limit of detection (3 s_B m^{-1}) of 0.03 μM.

Received 13th July 2020
Accepted 27th July 2020

DOI: 10.1039/d0ra06111e

rsc.li/rsc-advances

1 Introduction

Resorcinol or 1,3-dihydroxybenzene is an essential component in various industries including car tyre manufacturing,[1] wood bonding,[2] dermatological treatment,[3] hair dye production,[4] pharmaceuticals,[5] and organic synthesis.[6] Resorcinol is also found in fermenting bacteria,[7] and as the A-ring in flavonoids.[8] However, the uses of resorcinol come with significant toxicity risks to human health and the environment. The compound is highly soluble in water and can be easily released into the environment. Oral and skin exposure to resorcinol disrupts the performance of thyroid glands, central nervous systems and red blood cells.[9] Resorcinol consumption in pregnant women can lead to respiratory failure and the death of the fetus.[10] It is thus important to understand the physicochemical properties of resorcinol, and to have a fast and facile sensing method for resorcinol detection.

The oxidation of resorcinol is a complicated process, and controversy in its mechanistic pathway exists in literature. A number of reports suggest resorcinol oxidation to be an irreversible $2H^+$ $2e^-$ process forming 4-cyclohexene-1,3-dione as a product.[4,11–16] However, there is a lack of data to support the '$2H^+$ $2e^-$' mechanism. This mechanism arises from the experimental observation that the anodic peak potentials shifted with pH by *ca.* −59 mV pH^{-1} at 298 K.[11–16] The shift of −59 mV pH^{-1} indicates an equal number of proton(s) and electron(s) transferred during the oxidation process.[17] The exact number of the proton(s) and electron(s) involved in the oxidation, however, cannot be concluded from this data alone.

As quinones are formed in the $2H^+$ $2e^-$ oxidation of catechol (1,2-dihydroxybenzene) and hydroquinone (1,4-dihydroxybenzene),[18] similar reaction pathway has been anticipated for the oxidation of resorcinol. However, the oxidation of resorcinol is significantly different from that of catechol and hydroquinone, including the reversibility of the process and the characteristics of the electrochemical responses.[11,15,16] Catechol oxidation, for example, has the value of apparent transfer coefficient ($n' + \beta_{n'+1}$) between 1 and 2, and thus provides a strong evidence for a two-electron process with the second-electron transfer being the rate determining step.[18] However, we will demonstrate in this work that it is not the case for

[a]*School of Chemistry, Institute of Science, Suranaree University of Technology, 111 University Ave, Muang District, Nakhon Ratchasima, 30000, Thailand. E-mail: kamonwad@sut.ac.th; Tel: +66 44 224 637*

[b]*National Nanotechnology Center, National Science and Technology Development Agency, 111 Thailand Science Park, Pathum Thani, 12120, Thailand*

[c]*Research Network NANOTEC – SUT on Advanced Nanomaterials and Characterization, School of Chemistry, Suranaree University of Technology, Thailand*

† Electronic supplementary information (ESI) available: Electrode characterization; successive voltammetric scans; shifting of solvent breakdown potentials; calibration curve of resorcinol: cyclic voltammetry measurements. See DOI: 10.1039/d0ra06111e

resorcinol. Although the energetic stability of 4-cyclohexene-1,3-dione is consistent with the irreversibility of resorcinol oxidation,[11] the formation of quinone is not the only possible pathway for resorcinol oxidation.

Another possible pathway for resorcinol oxidation involves the formation of radical intermediates, which then proceed to form dimer/polymer products.[19,20] This mechanism is supported by the decrease in the anodic peak size in successive scans due to the fouling of the electrode after the deposition of polymeric films.[19,20] This reaction pathway has not been studied in detail, and will thus be investigated herein alongside the quinone formation route. However, the mechanism of resorcinol oxidation is very complex and cannot be deduced from experimental results alone. The reaction energies of elementary steps have to be considered in order to justify the most favorable reaction pathway. The primary aim of this work is thus to elucidate the mechanism of resorcinol oxidation by employing both DFT calculation and cyclic voltammetry experiments.

Importantly, different electrode materials have been used to study the irreversible behavior of resorcinol oxidation by electrochemical measurements.[11–16,21–28] The interaction between resorcinol and the electrode surface is influenced by the structure, morphology and electrocatalytic activity of the electrode material. The computational and experimental tools must be used as a novel alternative to understand the electrochemical oxidation–reduction mechanisms at different electrode surfaces. The elucidation of the reaction mechanisms would allow further development of various electrochemical applications including environmental monitoring and treatment, toxicity studies, as well as synthetic applications.[11–16,19,29–32]

In this work, the understanding of the oxidation process of resorcinol further leads to the development of an electrochemical sensor at a carbon microfiber electrode. To date, a number of electrochemical methods have been developed for resorcinol detection.[12,21–23,26,27] However, electrochemical measurements at conventional macroelectrodes, including those modified electrodes where macroscale substrates are used, are limited by the need of a large excess of supporting electrolytes to prevent ohmic drop effects, making it inconvenient for on-site applications.[24,25,28,33,34] At microelectrodes, the small magnitude of currents allow the requirement of supporting electrolyte to be significantly relaxed.[35–37] In this work, an electrochemical sensor for resorcinol detection is thus developed *via* the use of microelectrodes, and applied to low ionic strength samples.

2 Methods

2.1 Chemical reagents

All chemical reagents were of analytical grades and used as received without further purification: resorcinol (1,3-dihydroxybenzene, 99%, Sigma-Aldrich), hydrochloric acid (HCl, 37%, Sigma-Aldrich), sodium hydroxide (NaOH, ≥97.0%, Sigma-Aldrich), sodium phosphate dibasic (Na_2HPO_4, ≥99.0%, Sigma-Aldrich), sodium phosphate monobasic (NaH_2PO_4, ≥99.0%, Sigma-Aldrich), and potassium chloride (KCl, ≥99.0%, Sigma-Aldrich).

Buffer solutions were freshly prepared as follows: pH 1.0 – hydrochloric acid (HCl), pH 4.0 – citric acid/sodium citrate, pH 6.0 – sodium phosphate monobasic (NaH_2PO_4)/sodium phosphate dibasic (Na_2HPO_4), pH 9.0 – sodium carbonate (Na_2CO_3)/sodium bicarbonate ($NaHCO_3$), pH 10.0 – sodium bicarbonate ($NaHCO_3$) and sodium hydroxide (NaOH), pH 12.0, 13.0, 14.0 – sodium hydroxide (NaOH). The ionic strengths of all buffer solutions were adjusted to 0.10 M by the addition of potassium chloride (KCl).

2.2 Electrochemical measurement

Cyclic voltammetry (CV) and differential pulse voltammetry (DPV) experiments were performed with a PalmSens4 potentiostat (PalmSens, Netherlands) and an Autolab PGSTAT302N potentiostat (Metrohm, Netherlands) respectively, using a standard three electrode setup in a Faraday cage thermostated at 25 °C. A glassy carbon macrodisc (3.0 mm diameter, ItalSens) or a carbon fiber microdisc (7 μm diameter, BASi) was used as a working electrode. The working electrodes were polished on a water–alumina slurry (Buehler, USA) on soft lapping pads (Buehler, USA) prior to use. The working electrodes were then characterized by a standard redox probe, hexacyanoferrate(II)/hexacyanoferrate(III) ($Fe(CN)_6^{4-}/Fe(CN)_6^{3-}$) in the presence of 0.10 M potassium chloride (KCl) electrolyte; refer to Section S1 in the ESI.† A platinum sheet was used as a counter electrode. A silver/silver chloride (Ag/AgCl in 3.4 M KCl, ItalSens) or a silver wire was used as a reference electrode. All solutions were deoxygenated by a strong flow of nitrogen gas into the samples for 5 minutes to prevent interferences from oxygen reduction.

2.3 Computational detail

Quantum chemical calculations were carried out using the density functional theory (DFT)[38] method as implemented in the TURBOMOLE version 7.3 program package.[39] The effects of exchange and correlation were described by Becke's 3-parameter hybrid exchange-correlation functional, B3LYP.[40,41] The triple-zeta basis set with polarization function (TZVP) was used.[42] A self-consistent-field energy convergence criterion was set to 1.0×10^{-6} hartree and the standard grid (m3) for numerical quadrature was used.[43] Effects of water solvent ($\varepsilon = 80.40$) toward the optimized structures and their total energies were treated using the COSMO (conductor-like-screening model) approach.[44,45]

To systematically explore the mechanisms of resorcinol oxidation, we calculated reaction energies of all considered elementary steps including two types of reactions *i.e.* electron and H^+ abstractions. Reaction energies of the former, the oxidation energies, were calculated as the energy difference between two optimized intermediates where the product state has one less number of electron than that of the reactant state. The energy of H^+ abstraction processes were computed as, $(E_P + E_{H^+}) - E_R$, where E_P and E_R are the calculated total energies of product and reactant states, respectively. Note that the product state possesses one less number of the H atoms in the structure. The energy of H^+, E_{H^+}, was obtained from the reaction $H_2O + H^+ \rightarrow H_3O^+$. The potential energy profiles of most energetically favorable pathways were

constructed based on the calculated reaction energies of considered elementary steps.

3 Results and discussion

This work started with the voltammetric studies of resorcinol oxidation at macro- and micro-electrodes. We next performed DFT calculation to gain further insights into the mechanism of resorcinol oxidation and explore the most favourable reaction pathway. Following the understanding of the reaction mechanism, an electrochemical sensor was developed for resorcinol detection and the method was applied to low ionic strength samples.

3.1 Cyclic voltammetry at macroelectrodes

Resorcinol oxidation was first investigated experimentally by cyclic voltammetry at glassy carbon macroelectrodes. The aim of this study was to determine the chemical and electrochemical reversibility, the number of protons and electrons transferred, as well as the relevant kinetic parameters of resorcinol oxidation. For this purpose, cyclic voltammetry of resorcinol oxidation was performed at different scan rates and pH conditions before subjected to relevant analyses, detailed below.

3.1.1 Effects of pH. The solutions of 1.0 mM resorcinol in 0.10 M aqueous buffer solutions ($1 \leq pH \leq 14$) were subjected to cyclic voltammetry measurement ($E = 0.0 \rightarrow 1.4 \rightarrow 0.0$ V *vs.* Ag/AgCl [3.4 M KCl]) at the scan rate of 100 mV s^{-1}. The resulting voltammograms exhibited anodic peaks, corresponding to the oxidation of resorcinol (Fig. 1a). At pH $\geq$ 12, additional broad anodic peaks occurred at potentials near the onset of solvent breakdown. This broad peak became pronounced at high concentrations of hydroxide ions, and had been suggested to be the oxidation caused by oxygen radicals such as $OH^{\bullet}$ generated at high potentials.[19] No cathodic peaks were observed at all pH, indicating the electrochemically irreversible and/or chemically irreversible nature of the process, further evaluated later in the text.

As the pH of the solutions increased, the anodic peaks of resorcinol shifted towards lower potentials. The negative shift with pH indicated a deprotonation process associated with the removal of electron(s) from resorcinol to form a radical intermediate. To determine the number of H^+ and e^- involved, the peak potentials (E_p) were plotted against pH in Fig. 1b. Overall, the E_p *vs.* pH plot was non-linear. However, the graph can be divided into three sections separated by pK_{a1} (9.31)[9] and pK_{a2} (11.06)[9] of resorcinol in consideration of the different protonated states of the starting material.[18] In this work, we focused on the mechanisms at the two extreme pH ranges (pH < pK_{a1} and pH > pK_{a2}). At pH < pK_{a1}, the E_p *vs.* pH slope was determined to be -54 mV pH^{-1} close to the values previously reported for this pH range.[24] The results thus indicate an equal number of proton(s) and electron(s) in the oxidation of resorcinol ($ne^- nH^+$). At pH > pK_{a2}, no pH dependence was observed, consistent with the reactant (resorcinol) being in the deprotonated state prior to the start of the oxidation reaction.

3.1.2 Tafel analysis. The cyclic voltammetry results were next subjected to Tafel analysis (eqn (1)):[17,46]

$$\frac{\partial \ln I}{\partial E} = \frac{(n' + \beta_{n'+1})F}{RT} \quad (1)$$

where I is the electrical current, and E is the applied potential. n' is the number of electrons transferred before the rate determining electron transfer step, $\beta_{n'+1}$ is the anodic transfer coefficient of the rate determining electron transfer step, R is the molar gas constant (8.314 J K^{-1} mol^{-1}), T is the absolute temperature (K), and F is the Faraday constant (96 485 C mol^{-1}).[17] Only the currents in the range of 15–50% of the peak currents were considered for Tafel analysis to avoid the influence of diffusional mass transport.

From Tafel analysis in Fig. 2, the $n' + \beta_{n'+1}$ values for all pH were determined to be 0.6 ± 0.1. The results thus infer that $n' = 0$, and can be interpreted in three ways. First, the oxidation of resorcinol is an electrochemically irreversible one-electron transfer process. Second, it is a multi-electron process with the first electron transfer being the rate-determining step. Third, it is a multi-electron process with the true value of $n' + \beta_{n'+1}$ greater than 1, but the value is hindered by electrode fouling during the voltammetric scan. These hypotheses will be compared with the DFT results and returned to later in the text.

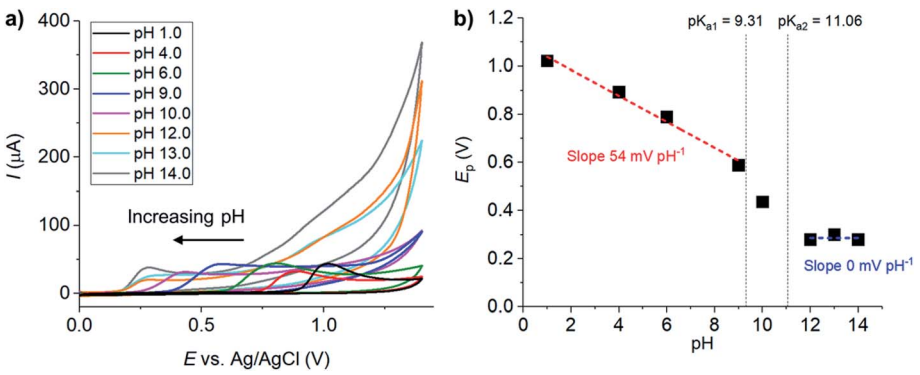

Fig. 1 (a) Cyclic voltammograms of 1.0 mM resorcinol at a glassy carbon macroelectrode (3.0 mm diameter) at the scan rate of 100 mV s^{-1} in various pH solutions. (b) A plot of the anodic peak potentials (E_p) against pH.

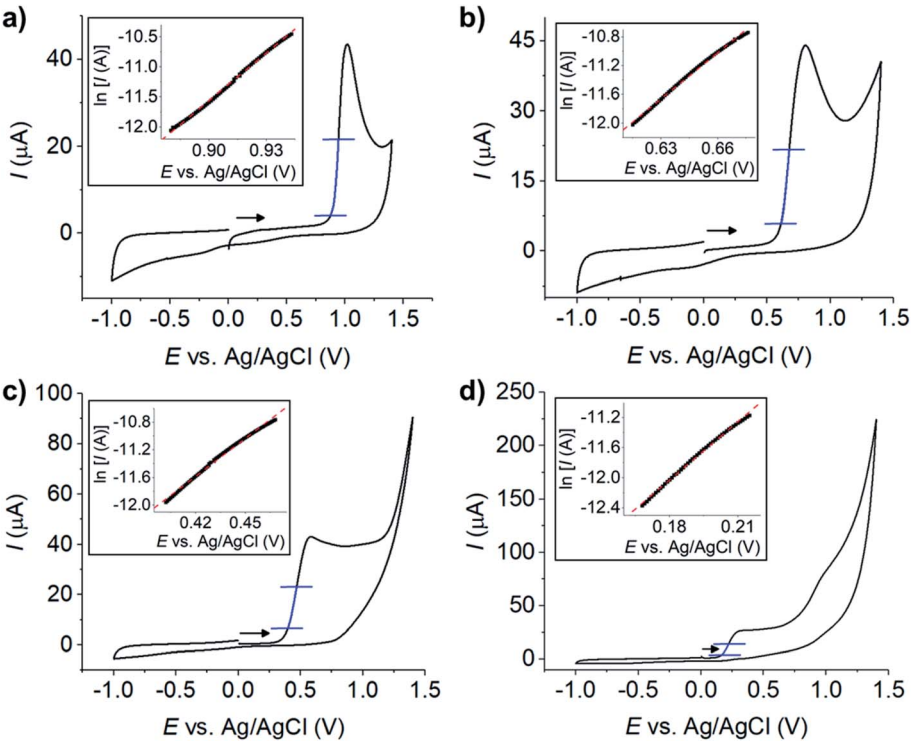

Fig. 2 Cyclic voltammograms of 1.0 mM resorcinol at a macroelectrode the scan rate of 100 mV s^{-1} at the pH of (a) 1.0; (b) 6.0; (c) 9.0; (d) 13.0. The blue lines indicate 15–50% of the peak currents used for Tafel analyses. Inlays: the Tafel plots of ln |*I*| against *E*.

3.1.3 Effects of scan rates. Resorcinol oxidation was further subjected to voltammetric studies at varied scan rates (10–400 mV s^{-1}) at a glassy carbon macroelectrode, refer to Fig. 3a for the results in pH 6.0 buffer. The peak position shifted towards more positive potentials as the scan rate (υ) increased, characteristics of an electrochemically irreversible process. The plot of E_p against log υ (inlay, Fig. 3a) gives the slope of 66.8 mV per decade of log υ.

The plot of the peak currents (I_p) against square root of scan rates ($\sqrt{\nu}$) is linear and passes through the origin (Fig. 3b). The process is thus diffusion controlled. The results agreed with previous experimental reports, as well as theoretical studies of activation energy being lower than 40 kJ mol^{-1}, indicating a diffusion-controlled process.[47] Notably, we have shown in our previous work that the adsorption of resorcinol can take place at a carbon surface. However, the adsorption process is very slow and has negligible effect on the voltammetric responses in the timescale of the experiments herein.

The diffusion coefficient of resorcinol can be estimated by eqn (2):

$$I_p = 0.496\sqrt{n' + \beta_{n'+1}}nFAc^*\sqrt{\frac{F\nu D}{RT}} \quad (2)$$

to be $5.2 \times 10^{-10} \pm 0.1 \times 10^{-10}$ m^2 s^{-1}, given that $\beta = 0.6$ (from Tafel analysis) $n' = 0$, $n = 1$, c^* is the bulk concentration of

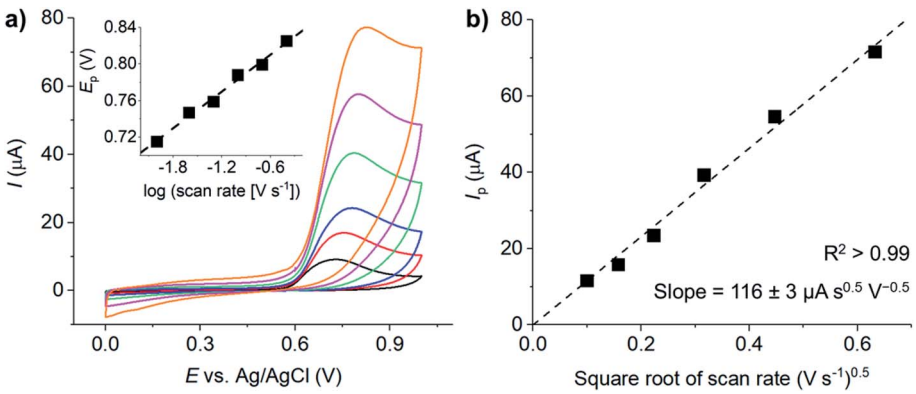

Fig. 3 (a) Cyclic voltammetry of 1.0 mM resorcinol in 0.10 M phosphate buffer pH 6.0 at a glassy carbon macroelectrode (3.0 mm diameter). Scan rates of 10–400 mV s^{-1}. (b) A plot of peak currents (I_p) *vs.* square root of scan rates (ν).

resorcinol ($c^* = 1.0$ mM), A is the electrode surface area ($A = 7.07$ mm^2), R is the molar gas constant (8.314 J K^{-1} mol^{-1}) and T is the absolute temperature under experimental conditions ($T =$ 298 K).

3.2 Cyclic voltammetry at microelectrodes

The oxidation of resorcinol was next investigated by cyclic voltammetry at microelectrodes to confirm its electrochemical behaviour and elucidate further insights into the process. Fig. 4a presents the voltammograms of 1.0 mM resorcinol oxidation in 0.10 M aqueous buffers ($1 \leq$ pH ≤ 14) at a carbon microdisc electrode (7 μm diameter) at the scan rate of 10 mV s^{-1}. Interestingly, peak-shaped responses were observed. The currents did not reach steady state even though a microelectrode was used, and the voltammetry conducted at the slow scan rate of 10 mV s^{-1}. These results are consistent with the formation of an electrochemically inert products on the surface of the electrode.

The formation of inert film on the electrode was further evidenced by the following experiments. Successive voltammetric scans of resorcinol oxidation were performed using the same electrode without electrode polishing between scans. The diffusion layers were refreshed by solution stirring before each scan. An anodic peak of resorcinol oxidation was observed in the first scan as usual. However, no oxidation peak was observed in the following scans. After careful polishing, the electrode regained its electroactivity, and thus evidenced the fouling of the electrode surface upon the oxidation of resorcinol (Fig. S2, ESI†).

The effects of pH on the cyclic voltammetry responses of resorcinol oxidation at microelectrodes were studied next. The resulting voltammograms showed irreversible anodic peaks associated with the oxidation of resorcinol, while cathodic peaks were absent at all pH (Fig. 4a). The position of the anodic peaks shifted towards lower potentials as the pH of the solutions increased, similar to the results at macroelectrodes. The plot of the peak potential (E_p) against pH in Fig. 4b was non-linear, and was divided into three sections separated by the pK_a's of resorcinol. When the solution was more acidic than pK_{a1} of resorcinol, the E_p *vs.* pH slope was −52.2 mV pH^{-1}, close to the value at a macroelectrode. The oxidation of resorcinol then became independent of pH when the solution was more basic than the pK_{a2} of resorcinol, again agreed with the results at macroelectrodes. We also found that solvent breakdown shifted to higher overpotentials in the presence of resorcinol (Fig. S3, ESI†).

Tafel analysis of resorcinol cyclic voltammetry at microelectrodes was also attempted. Background subtraction (voltammogram of resorcinol oxidation – voltammogram of blank buffer solution) was considered. However, significant deviations from linearity of the ln I (15–50% of I_p) *vs.* E plot were observed with and without background subtraction. At microelectrodes, diffusional mass transport had greater influence on the voltammetric responses than macroelectrodes. In this case, there were also complications from the irreversible formation of polymeric film, and the unusual voltammetric peak shapes. Therefore, transfer coefficients could not be determined with sufficient accuracy at microelectrodes.

3.3 Mechanistic studies by DFT calculation

To obtain insights into the mechanism of resorcinol electrooxidation in aqueous solution, we utilized the DFT method to explore the most favorable pathways. The electrochemical reaction in the solution is expected to be very complex. For simplicity, we employed the implicit solvation model of COSMO method and calculated the energies of the optimized intermediates in the absence of other compounds. To systematically investigate the oxidation mechanism, we considered various possible reaction pathways where both abstractions of an electron and H$^+$ were included in a stepwise fashion, as shown in Fig. 5. The favorable pathways were determined from the reaction energy of each elementary step which can be calculated as the difference of total energy of the optimized intermediates. In addition, the eigenvalues of highest occupied molecular orbital (HOMO) of intermediates can be used to suggest the tendency to lose electrons where the higher the HOMO energy the easier it is to give away an electron.

As shown in Fig. 5, computations reveal that in order to form the oxidized monomer (4-cyclohexene-1,3-dione, RS10), it is energetically more favorable for resorcinol reactant to first lose

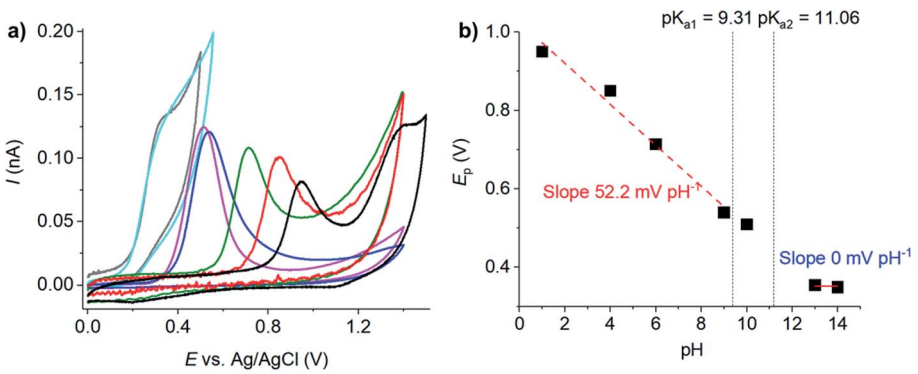

Fig. 4 (a) Cyclic voltammograms of 1.0 mM resorcinol at a carbon microelectrode (7 μm diameter) at the scan rate of 10 mV s^{-1} in various pH solutions. (b) A plot of the anodic peak potentials (E_p) against pH.

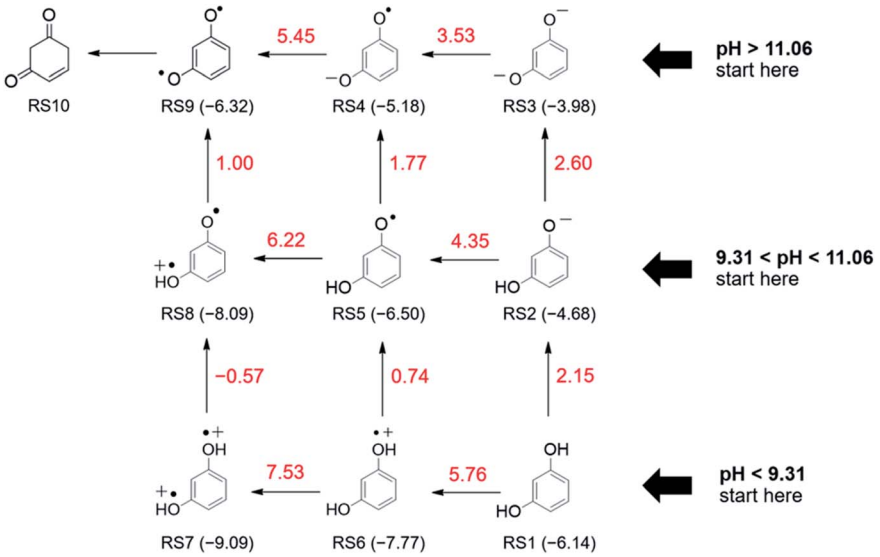

Fig. 5 Scheme of squares of resorcinol oxidation. The numbers in parentheses represent HOMO energies of each species. The reaction energies of each considered elementary steps are labeled as red numbers. All energies are in eV.

its H^+ prior getting oxidized. As for the first step, the abstraction of H^+ requires much less energy (RS1 → RS2, 2.15 eV) than that of the direct oxidation (RS1 → RS6, 5.76 eV). Likewise, the obtained RS2 intermediate prefers to sacrifice its H^+ (2.60 eV) than to lose its electron (4.35 eV). Then, the deprotonated intermediate, RS3, undergoes oxidation where two electrons are withdrawn from the RS3 ion resulting in the RS9 intermediate with a rather high net reaction energy of 3.53 + 5.45 = 7.98 eV. The calculated HOMO eigenvalues provide insight into the energetically preferred reaction pathway. It can be seen that the HOMO energies of the intermediates are increased upon H^+ abstraction indicating the increased oxidizability of the intermediates. The reaction energy of first electron oxidation is decreased from 5.76 eV to 4.35 eV after a H^+ abstraction and further reduced to 3.53 eV when it loses two H^+.

In addition, our electrochemical experiments indicate formation of polymeric film on the microelectrode. Hence, it is of our particular interest to computationally explore the alternative mechanism of polymer formation *via* radical formation route, Fig. 6a. Resorcinol oxidation can yield active monomer radicals that leads to the formation of various polymers. Among the considered radicals in this study, the RS5 intermediate is energetically feasible to occur as it requires less energy (RS2 → RS5, 4.35 eV) to get oxidized than that for the other radicals, Fig. 5. Formation of the RS5 radical follows similar reaction pathway as described above (RS1 → RS2 → RS5). The generated RS5 radical, whose unpaired electron is localized on the oxygen atom, can subsequently isomerize to have its radical on the carbon ring, RS11. This isomerization process, RS5 → RS11 (Fig. 6a), is energetically uphill by 1.30 eV which is consistent with the previously calculated value (1.31 eV).[48] From the energy profile depicted in Fig. 6a, the radical formation route, branched from the monomer oxidation route, is more favorable as it does not require the loss of the second electron (RS4 → RS9) which is energetically much more demanding. The generated radicals, *e.g.* RS5 and RS11, can readily react to form dimers as shown in Fig. 6b. As expected, formation of dimers from the active radicals are exothermic where the dimer products are significantly more stable. Possible dimer products are demonstrated in Fig. 6b. These dimers can further react to form polymers which cover the electrode surface and cause electrode deactivation.[49] Overall, the calculated results are consistent with our experimental studies that the electro-oxidation of resorcinol is indeed a one-electron process where the reaction mainly produces polymers covered on the electrode surfaces.

From the results of both experimental and computational studies, we thus conclude that the electro-oxidation of resorcinol is electrochemically and chemically irreversible. At pH < pK_{a1}, the first step in resorcinol oxidation is a $1H^+$ deprotonation associated with an irreversible removal of $1e^-$ to form a radical (RS5). At pH > pK_{a2}, the process becomes independent of pH. The first step under this condition is thus the removal of $1e^-$ to form the RS4 radical. The radicals then proceed to form dimers/polymers in an exothermic process. From the cyclic voltammetry results, we showed that the final product of resorcinol oxidation is electrochemically inert as evidenced by the peak-shaped responses (*i.e.* not steady state) at a microelectrode and the fouling of the electrode. We also showed that this electrochemically inert product is deposited on the electrode surface from the results of successive voltammetric scans. Once the low-energy dimer/polymer is formed, the system becomes highly stable and does not undergo a backward reduction reaction, resulting in the absence of the cathodic peak in the voltammetry. In addition to being thermodynamically stable as confirmed by the DFT studies, the absence of the cathodic peak could be due to the polymeric film being non-conductive and thus experienced significant ohmic drop across the electrode surface.

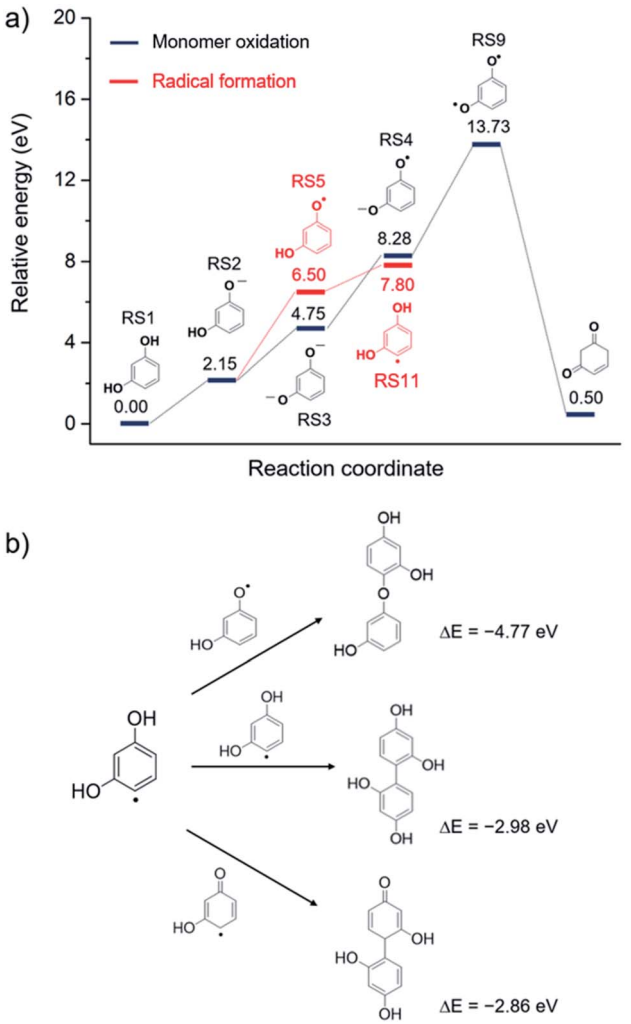

Fig. 6 (a) Potential energy profiles constructed using the reaction energies of the two possible pathways: monomer oxidation (black) and radical monomer formation (red) where (b) the formed radicals effectively react to generate various stable dimer products.

3.4 Sensing application: resorcinol detection in low ionic strength samples

Having gained insights into the process of resorcinol oxidation, we next explore its analytical applications. At conventional macroelectrodes, a large amount of supporting electrolyte (usually 100 times of the analyte's concentration) is needed to avoid ohmic drop effects. Below, we studied the differences in the voltammetric responses of resorcinol oxidation at macro- and micro-electrodes in the absence of supporting electrolytes. To prevent the leakage of salt into the solutions, a silver wire was used as a pseudo reference electrode. The conductivity of air equilibrated deionized water employed in the experiments was measured to be 1.4 μS cm^{-1}. The measured conductivity is higher than the value stated inside the water producing machine due to the dissolution of atmospheric CO_2 to form ionic species such as HCO_3^- and H^+,[50] making the solution sufficiently conductive for electrochemical measurements at microelectrodes.

Fig. 7 compares normalized cyclic voltammograms of 1.0 mM resorcinol in deionized water at a macroelectrode *vs.* a microelectrode in the absence of supporting electrolytes at the scan rate of 10 mV s^{-1}. At a macroelectrode, the anodic peak of resorcinol oxidation was absent. Meanwhile, resorcinol could be easily detected voltammetrically at a microelectrode without any significant ohmic distortion. We thus clearly demonstrated the advantage of microelectrodes in resorcinol detection in low ionic strength samples.

The solutions of varied resorcinol concentrations were next subjected to cyclic voltammetry and differential pulse voltammetry at a microelectrode in the absence of supporting electrolytes. As compared to cyclic voltammetry (Section S4, ESI†), differential pulse voltammetry enhanced the oxidative responses of resorcinol oxidation due to the minimized capacitative (background) currents. The differential pulse voltammograms are demonstrated in Fig. 8. The inlay in Fig. 8 showed the calibration plot of the peak currents (I_p) against resorcinol concentrations, with the sensitivity of 123 ± 4 nA μM^{-1} and the limit of detection (3 s_B m^{-1}) of 0.03 μM. This value of limit of detection is comparable to that of various modified electrodes presented in the literature.[11–16,21–28]

The ability of microelectrodes to give well-defined electrochemical responses in low ionic strength samples allow direct detection of resorcinol in a single step without the need for sample preparation or electrode modification. The sub-micromolar limit of detection would allow the application of the method in a wide range of samples which contain micromolar levels of resorcinol such as hair dyes, urine, blood serum and water resources.[4] The possible limitations of the method lie in the possibility of electrode fouling due to the formation of inert polymeric films on the electrode surface. Polishing or electrochemical cleaning of the electrode surface is thus required. There are also possibility of interference effects in very complex systems. However, the advantages of electrochemical sensors such as short measurement time, low-cost instrumentation and high sensitivity outweigh these limitations. The method is particularly suitable for quick screening tests or in situations where a large number of samples have to be tested in a short time.

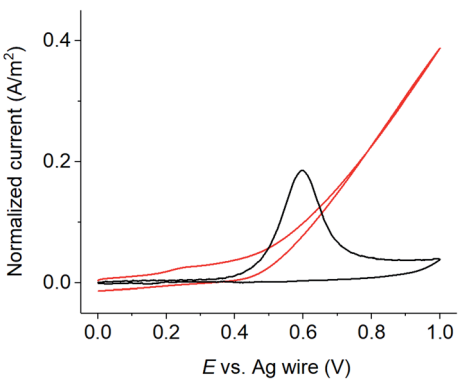

Fig. 7 Cyclic voltammetry of 1.0 mM resorcinol at a carbon microelectrode in the absence of added electrolytes. Scan rate of 10 mV s^{-1}.

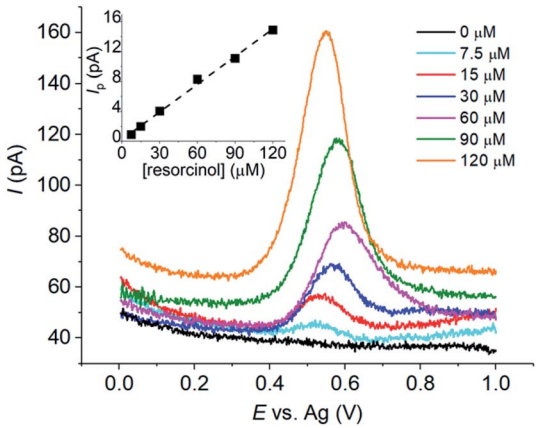

Fig. 8 Differential pulse voltammograms of varied concentrations of resorcinol in deionized water at a carbon microelectrode (7 μm diameter); step potential = 0.001 V, modulation (pulse) amplitude = 0.050 V, modulation time = 0.050 s, interval time = 0.1 s. The inlay shows the calibration plot of the peak currents against resorcinol concentrations.

4 Conclusions

The oxidation of resorcinol was evaluated by both DFT calculation and cyclic voltammetry measurements at macro- and micro-electrodes. All of the experimental findings agreed with the DFT results that resorcinol oxidation proceeded *via* an electrochemically irreversible $1H^+$ $1e^-$ process, followed by the irreversible formation of electrochemically inert polymers. Similar mechanistic pathway was proposed for resorcinol oxidation in very basic solutions (pH > 11), except that there was no H^+ transfer taking place and the process became independent of pH. Finally, we further highlighted the ability of microelectrodes to detect resorcinol in low ionic strength samples, and thus provided a fast and facile sensing method for resorcinol detection.

Conflicts of interest

There are no conflicts to declare.

Acknowledgements

This work is supported by Suranaree University of Technology and the Research Network NANOTEC (RNN) program of the National Nanotechnology Center (NANOTEC), NSTDA, Ministry of Higher Education, Science, Research and Innovation (MHESI), Thailand. We would like to thank NSTDA Supercomputer Center (ThaiSC); and Institute of Science and the Center for Scientific and Technological Equipment, Suranaree University of Technology for computational resources.

References

1 H. Dressler, The Use of Resorcinol in Rubber Compositions, in *Resorcinol: Its Uses and Derivatives*, Springer US, Boston, MA, 1994, pp. 59–83.
2 C. B. Vick, K. H. Richter and B. H. River, Hydroxymethylated resorcinol coupling agent and method for bonding wood, *US Pat.*, 5543487, August 6, 1996.
3 A. W. Hinman, D. Davis and V. Kheifets, Resorcinol compounds for dermatological use, *US Pat.*, US 2016/0000669 A1, January 7, 2016.
4 G. Manasa, A. K. Bhakta, Z. Mekhalif and R. J. Mascarenhas, Voltammetric study and rapid quantification of resorcinol in hair dye and biological samples using ultrasensitive maghemite/MWCNT modified carbon paste electrode, *Electroanalysis*, 2019, **31**(7), 1363–1372.
5 M. R. Gomez, R. A. Olsina, L. D. Martínez and M. F. Silva, Simultaneous determination of cloramphenicol, salicylic acid and resorcinol by capillary zone electrophoresis and its application to pharmaceutical dosage forms, *Talanta*, 2003, **61**(2), 233–238.
6 M. Albrecht, J. Zauner, R. Fröhlich, O. Kataeva, E. Wegelius and K. Rissanen, Tweezer-type catechol and resorcinol derivatives: Preparation, structures, and first investigations towards their hydrogen bonding abilities, *Synthesis*, 2002, **2002**(10), 1434–1444.
7 C. Kluge, A. Tschech and G. Fuchs, Anaerobic metabolism of resorcyclic acids (*m*-dihydroxybenzoic acids) and resorcinol (1,3-benzenediol) in a fermenting and in a denitrifying bacterium, *Arch. Microbiol.*, 1990, **155**(1), 68–74.
8 V. Castaignède, H. Durliat and M. Comtat, Amperometric and Potentiometric Determination of Catechin as Model of Polyphenols in Wines, *Anal. Lett.*, 2003, **36**(9), 1707–1720.
9 S. Hahn, J. Kielhorn, J. Koppenhöfer, A. Wibbertmann and I. Mangelsdorf, *Concise International Chemical Assessment Document 71*, World Health Organization: Geneva, Switzerland, 2006.
10 B. Duran, S. Gursoy, M. Cetin, N. Demirkoprulu, Y. Demirel and B. Gurelik, The oral toxicity of resorcinol during pregnancy: a case report, *J. Toxicol., Clin. Toxicol.*, 2004, **42**(5), 663–666.
11 A. R. L. da Silva, A. J. dos Santos and C. A. Martínez-Huitle, Electrochemical measurements and theoretical studies for understanding the behavior of catechol, resorcinol and hydroquinone on the boron doped diamond surface, *RSC Adv.*, 2018, **8**(7), 3483–3492.
12 S. M. Ghoreishi, M. Behpour, E. Hajisadeghian and M. Golestaneh, Voltammetric determination of resorcinol on the surface of a glassy carbon electrode modified with multi-walled carbon nanotube, *Arabian J. Chem.*, 2016, **9**, S1563–S1568.
13 M. Khodari, Electrochemical Sensor based on Carbon Paste Electrode Modified by TiO_2 nano-particles for the voltammetric determination of resorcinol, *Int. J. Electrochem. Sci.*, 2018, 3460–3474.
14 H. Hammani, F. Laghrib, A. Farahi, S. Lahrich and M. El Mhammedi, Catalytic Effect of Activated Carbon in Determining Resorcinol in Water and Hair Color at Graphite Electrode, *Waste Biomass Valorization*, 2020, 1–12.
15 L. Huang, Y. Cao and D. Diao, Electrochemical activation of graphene sheets embedded carbon films for high sensitivity

simultaneous determination of hydroquinone, catechol and resorcinol, *Sens. Actuators, B*, 2020, **305**, 127495.

16 Y. Zhang, Q. Xie, Z. Xia, G. Gui and F. Deng, Graphdiyne oxides as new modifier for the simultaneous electrochemical detection of phenolic compounds, *J. Electroanal. Chem.*, 2020, 114058.

17 R. G. Compton and C. E. Banks, *Understanding voltammetry*, World Scientific, 2011.

18 Q. Lin, Q. Li, C. Batchelor-McAuley and R. G. Compton, Two-electron, two-proton oxidation of catechol: kinetics and apparent catalysis, *J. Phys. Chem. C*, 2015, **119**(3), 1489–1495.

19 B. Nasr, G. Abdellatif, P. Canizares, C. Sáez, J. Lobato and M. A. Rodrigo, Electrochemical oxidation of hydroquinone, resorcinol, and catechol on boron-doped diamond anodes, *Environ. Sci. Technol.*, 2005, **39**(18), 7234–7239.

20 H. Nady, M. El-Rabiei and G. A. El-Hafez, Electrochemical oxidation behavior of some hazardous phenolic compounds in acidic solution, *Egypt. J. Pet.*, 2017, **26**(3), 669–678.

21 Y.-P. Ding, W.-L. Liu, Q.-S. Wu and X.-G. Wang, Direct simultaneous determination of dihydroxybenzene isomers at C-nanotube-modified electrodes by derivative voltammetry, *J. Electroanal. Chem.*, 2005, **575**(2), 275–280.

22 Z. Wang, S. Li and Q. Lv, Simultaneous determination of dihydroxybenzene isomers at single-wall carbon nanotube electrode, *Sens. Actuators, B*, 2007, **127**(2), 420–425.

23 H. D. R. Manjunatha, Electrochemical Investigation of Resorcinol in Pterocarpus marsupium RoxB by Cyclic Voltammetric Study, *J. Anal. Bioanal. Tech.*, 2014, **5**(6), 218.

24 H. Yin, Q. Zhang, Y. Zhou, Q. Ma, T. liu, L. Zhu and S. Ai, Electrochemical behavior of catechol, resorcinol and hydroquinone at graphene–chitosan composite film modified glassy carbon electrode and their simultaneous determination in water samples, *Electrochim. Acta*, 2011, **56**(6), 2748–2753.

25 W. Zhang, J. Zheng, Z. Lin, L. Zhong, J. Shi, C. Wei, H. Zhang, A. Hao and S. Hu, Highly sensitive simultaneous electrochemical determination of hydroquinone, catechol and resorcinol based on carbon dot/reduced graphene oxide composite modified electrodes, *Anal. Methods*, 2015, **7**(15), 6089–6094.

26 D. Zhang, Y. Peng, H. Qi, Q. Gao and C. Zhang, Application of multielectrode array modified with carbon nanotubes to simultaneous amperometric determination of dihydroxybenzene isomers, *Sens. Actuators, B*, 2009, **136**(1), 113–121.

27 M. Arago, C. Arino, A. Dago, J. M. Diaz-Cruz and M. Esteban, Simultaneous determination of hydroquinone, catechol and resorcinol by voltammetry using graphene screen-printed electrodes and partial least squares calibration, *Talanta*, 2016, **160**, 138–143.

28 K.-J. Huang, L. Wang, Y.-J. Liu, T. Gan, Y.-M. Liu, L.-L. Wang and Y. Fan, Synthesis and electrochemical performances of layered tungsten sulfide-graphene nanocomposite as a sensing platform for catechol, resorcinol and hydroquinone, *Electrochim. Acta*, 2013, **107**, 379–387.

29 R. B. Durairaj, *Resorcinol: chemistry, technology and applications*. Springer Science & Business Media, 2005.

30 R. Guo, J. Guo, F. Yu and D. D. Gang, Synthesis and surface functional group modifications of ordered mesoporous carbons for resorcinol removal, *Microporous Mesoporous Mater.*, 2013, **175**, 141–146.

31 J. Huang, K. Huang and C. Yan, Application of an easily water-compatible hypercrosslinked polymeric adsorbent for efficient removal of catechol and resorcinol in aqueous solution, *J. Hazard. Mater.*, 2009, **167**(1–3), 69–74.

32 L. Zhang, H. Liu, M. Wang and L. Chen, Structure and electrochemical properties of resorcinol–formaldehyde polymer-based carbon for electric double-layer capacitors, *Carbon*, 2007, **45**(7), 1439–1445.

33 K. M. Hassan, A. A. Hathoot and M. A. Azzem, Simultaneous and selective electrochemical determination of hydroquinone, catechol and resorcinol at poly(1,5-diaminonaphthalene)/glassy carbon-modified electrode in different media, *RSC Adv.*, 2018, **8**(12), 6346–6355.

34 Z. Li, Y. Yue, Y. Hao, S. Feng and X. Zhou, A glassy carbon electrode modified with cerium phosphate nanotubes for the simultaneous determination of hydroquinone, catechol and resorcinol, *Microchim. Acta*, 2018, **185**(4), 215.

35 K. Ngamchuea, C. Batchelor-McAuley and R. G. Compton, Understanding electroanalytical measurements in authentic human saliva leading to the detection of salivary uric acid, *Sens. Actuators, B*, 2018, **262**, 404–410.

36 C. Batchelor-McAuley, K. Ngamchuea and R. G. Compton, Simulated low-support voltammetry: deviations from Ohm's Law, *J. Electroanal. Chem.*, 2018, **830**, 88–94.

37 K. Ngamchuea, C. Batchelor-McAuley and R. G. Compton, Anodic stripping voltammetry of silver in the absence of electrolytes: theory and experiment, *J. Electroanal. Chem.*, 2018, **830**, 122–130.

38 W. Kohn and L. J. Sham, Self-Consistent Equations Including Exchange and Correlation Effects, *Phys. Rev.*, 1965, **140**(4A), A1133–A1138.

39 R. Ahlrichs, M. Bär, M. Häser, H. Horn and C. Kölmel, Electronic structure calculations on workstation computers: the program system turbomole, *Chem. Phys. Lett.*, 1989, **162**(3), 165–169.

40 P. J. Stephens, F. J. Devlin, C. F. Chabalowski and M. J. Frisch, *Ab Initio* Calculation of Vibrational Absorption and Circular Dichroism Spectra Using Density Functional Force Fields, *J. Phys. Chem.*, 1994, **98**(45), 11623–11627.

41 R. H. Hertwig and W. Koch, On the parameterization of the local correlation functional. What is Becke-3-LYP?, *Chem. Phys. Lett.*, 1997, **268**(5), 345–351.

42 S. Kossmann and F. Neese, Comparison of two efficient approximate Hartee–Fock approaches, *Chem. Phys. Lett.*, 2009, **481**(4–6), 240–243.

43 O. Treutler and R. Ahlrichs, Efficient molecular numerical integration schemes, *J. Chem. Phys.*, 1995, **102**(1), 346–354.

44 A. Klamt and G. Schüürmann, COSMO: a new approach to dielectric screening in solvents with explicit expressions for the screening energy and its gradient, *J. Chem. Soc., Perkin Trans. 2*, 1993, **5**, 799–805.

45 J. Tomasi, B. Mennucci and R. Cammi, Quantum Mechanical Continuum Solvation Models, *Chem. Rev.*, 2005, **105**, 2999.
46 C. Batchelor-McAuley and R. G. Compton, Voltammetry of multi-electron electrode processes of organic species, *J. Electroanal. Chem.*, 2012, **669**, 73–81.
47 B. K. Körbahti and P. Demirbüken, Electrochemical oxidation of resorcinol in aqueous medium using boron-doped diamond anode: reaction kinetics and process optimization with response surface methodology, *Front. Chem.*, 2017, **5**, 75.
48 J. Hladyszowski, L. Zubik and A. Kozubek, Quantum mechanical and experimental oxidation studies of pentadecylresorcinol, olivetol, orcinol and resorcinol, *Free Radical Res.*, 1998, **28**(4), 359–368.
49 H. Yi, K. Wu, S. Hu and D. Cui, Adsorption stripping voltammetry of phenol at Nafion-modified glassy carbon electrode in the presence of surfactants, *Talanta*, 2001, **55**(6), 1205–1210.
50 X. Li, C. Batchelor-McAuley, E. Laborda and R. G. Compton, Aqueous voltammetry in the near absence of electrolyte, *Chem.–Eur. J.*, 2017, **23**(60), 15222–15226.